Simulation of scanning tunneling spectroscopy of supported carbon nanotubes

Géza I. Márk,[1,2,*] László P. Biró,[2,3] József Gyulai,[2] Paul A. Thiry,[3] Amand A. Lucas,[1] and Philippe Lambin[1]
[1]*Laboratoire de Physique du Solide, Facultés Universitaires Notre Dame de la Paix, 61, Rue de Bruxelles, B-5000 Namur, Belgium*
[2]*Research Institute for Technical Physics and Materials Science, H-1525 Budapest, P.O. Box 49, Hungary*
[3]*Laboratoire de Spectroscopie Moleculaire de la Surface, Facultés Universitaires Notre Dame de la Paix, 61, Rue de Bruxelles, B-5000 Namur, Belgium*
(Received 29 November 1999)

The angle and energy dependent transmission of wave packets was calculated through a jellium potential model of a scanning tunneling microscope (STM) junction containing different arrangements of carbon nanotubes. The total tunnel current as a function of STM bias was calculated by statistical averaging over a distribution of wave packets in the allowed energy window. Three tunneling situations were studied: (i) a STM tunnel junction with no nanotube present, (ii) one single wall nanotube in the STM junction, and (iii) a nanotube ''raft.'' The effects of point contacts at the STM tip/nanotube, at the nanotube/substrate, and at both interfaces were also investigated. The theory allowed us to identify components of pure geometrical origin responsible for the asymmetry in the scanning tunneling spectroscopy (STS) spectrum of the carbon nanotubes with respect to bias voltage polarity. The calculations show that for tip negative bias the angular dependence of the transmission is determined by the tip shape. The particular tip shape introduces an asymmetry on the negative side of the STS spectrum. For tip positive bias the angular dependence of the transmission depends strongly on the nature of the nanosystem in the STM gap. While the transmission of the STM tunnel junction with no nanotube present can be well represented by a one dimensional model, all other geometries cause a large normal-transverse momentum mixing of the wave packet. A diffraction-grating-like behavior is seen in the angular dependence of the transmission of the nanotube raft. Point contacts between the nanotube and the substrate cause an asymmetry in the positive side of the STS spectrum. Calculated STS spectra are compared to experimental ones.

I. INTRODUCTION

Single wall carbon nanotubes (SWCNTs) are objects composed of carbon with typical diameters of the order of 1 nm. The structure of a SWCNT is like that resulting after rolling a single sheet of graphene into a cylinder. The electronic properties of a SWCNT in the first approximation are determined by how this rolling is done.[1] Calculations based on a tight-binding Hamiltonian show that the gap value for a given SWCNT depends only on the value of its diameter,[2] which is unambiguously determined by the rolling vector $\vec{T} = n\vec{a}_1 + m\vec{a}_2$, where $\vec{a}_1$ and $\vec{a}_2$ are the lattice vectors of the graphene sheet.[3] A multiwall carbon nanotube (MWCNT) is built by placing smaller diameter SWCNTs in larger diameter ones concentrically in such a way that the graphene cylinders are separated by a distance of 0.34 nm. Another regular, multishell structure frequently found experimentally is the ''rope''[4] or ''raft''[5] of CNTs, which is built by placing the CNTs side by side in such a way that their axes are parallel to each other with intertube spacing 0.32 nm characteristic of van der Waals inter-SWCNT bonding.[4]

Because of to its ability to image objects with typical dimensions in the nanometer range, the scanning tunneling microsocpe (STM) is very well suited to investigate CNTs (see Ref. 6 for a recent review). In addition to topographic images, the electronic structure of CNTs can be probed by scanning tunneling spectroscopy (STS).[7–11] In order to be investigated by STM the CNTs have to be supported on an atomically flat conducting substrate, most frequently Au or highly oriented pyrolitic graphite (HOPG). In the interpretation of the STS data, one should take into account the complex structure of the system[12,13] through which the tunneling takes place. The simplest formalism used in interpretation of the STS data of single crystalline surfaces[14] is valid for describing the process of tunneling through a one dimensional potential barrier. On the other hand, no tractable formalism is available for analytically calculating the tunneling current from the STM tip to the support through a CNT. Therefore, the simulation of the tunneling process using a recently developed computer code[13] is helpful in the interpretation of experimental data.

A further effect that must be taken into account in the interpretation of STS data is the value of the tunneling gap between the tip and the imaged object. Early work on the dependence of STS spectra on the width of the tunneling gap showed that the STS results are influenced by this value.[15,16] This gap can be an important parameter in understanding the STS data and the topographic STM images of CNTs. Atomic resolution images of CNTs do not exclude the possibility of point contact imaging.[15] Recent results, based on computer modeling of atomic resolution STM images[17] compared to experimentally measured atomic resolution images, and to diameter values inferred from STS measurements, indicate anomalously small gap values between the SWCNT and the STM tip.[18]

Exploring the way that the current tunnels between a sharp tip and a CNT is not an easy task because of the complicated shape of the potential barrier.[19] This question is addressed in the present paper. The basic ideas and restrictions

of the method developed here are as follows. (i) The tunneling problem is regarded as a problem in potential scattering theory.[20–22] The current density is determined by calculating the scattering of wave packets (WPs) incident on the barrier potential. (ii) The method applies to localized barriers. By localized, we mean situations in which nonperiodic spatial variations of the potential occur only over a finite *interface region* of nanoscopic size. (iii) The initial WPs are constructed from the stationary states of the reservoir from which the WPs are arriving. The initial WP is formed in such a way that its envelope function will have a constant plateau of larger size than the spatial dimension of the interface region. (iv) The total tunnel current at a given STM bias is a statistical average of the tunnel currents for WPs of different allowed incident energies and directions ($\vec{k}$ vectors) weighted according to the band structure of the two reservoirs.

In this calculation focusing on geometric, point contact, and bias effects we used a simple jellium potential which does not take into account the atomic structure. As shown recently,[23] the self-consistent electronic structure of CNTs represented by the jellium background model compares favorably with parametrized linear combination of atomic orbitals calculations that take atomic structure into account. The absence of atomic structure in the jellium tubes is equivalent to averaging over all chiral angles. At this level of approximation, all CNTs are metallic. This means that our approach is unable to deal with semiconducting CNTs at low bias potential.

The calculations were done for a two dimensional (2D) barrier model. While this neglects some important effects, e.g., the spread of the charge along the tube, which may be important for metallic tubes, a 2D calculation with readily available computer resources makes it possible to explore the essential phenomena governing the incident angle dependence of transmission through supported nanostructures. Such phenomena cannot be studied in the framework of 1D models. In the detailed discussion below we always note when 3D effects are expected to modify a particular feature qualitatively.

In the present paper the effects arising from tip geometry and tip polarity are investigated. Furthermore, the possible effects of point contact at the STM tip/CNT, at the CNT/substrate, and at both interfaces are modeled. The effect produced by placing regular arrangements (rafts) of CNTs under the STM tip are simulated. The raft geometry is used to mimic an ordered two dimensional array of nanotubes on a flat substrate. It is assumed that the intertube interaction in CNT rafts is similar to that found in nanotube ropes.

The organization of the paper is as follows. In Sec. II the tunnel barrier is constructed for an STM junction containing the different arrangements of CNTs and point contacts. Section III gives an outline of the wave packet dynamical method of calculating the tunnel current. In Sec. IV numerical results are presented for the angle and energy dependence of the transmission probability and for the tunnel current as a function of STM bias. Section V is devoted to discussion of the results.

Hartree atomic units are used in all formulas unless where explicit units are given. SI units are used, however, in all the figures and numerical data.

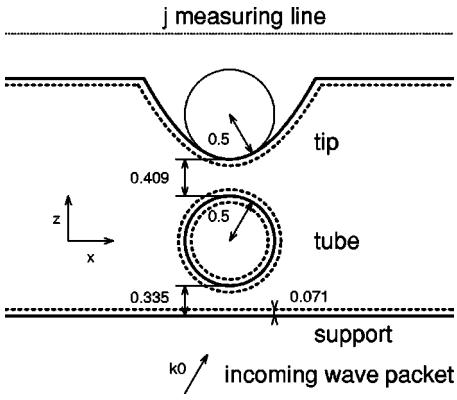

FIG. 1. Model system. The lower half plane, middle ring, and hyperbolic protrusion on the upper half plane show the vertical cross sections of the support, nanotube, and tip, respectively. The effective surface (broken line) is 0.071 nm outside the geometric surface (full line). The arrow labeled k_0 shows the incidence direction of the incoming wave packet. $\vec{j}_{prob}$ is measured along the dotted line in the tip bulk. The particular wave packet and measuring line position is for a tip positive situation. In the tip negative case the wave packet is approaching the tunnel junction from the tip bulk and $\vec{j}_{prob}$ is measured in the support bulk. All dimensions are in nomometers.

II. BARRIER MODEL

The model system is shown in Fig. 1. It is infinitely long in the y direction. The geometrical and material parameters of the CNT and the tip are the same as in Ref. 13. The CNT is modeled by a cylinder of 0.5 nm radius floating above the support at a distance of 0.335 nm. The STM tip is taken as a hyperbolic cylinder of 0.5 nm apex radius and 15° aperture angle. The effective surface of these objects is assumed to be 0.071 nm outside their geometric surface (defined as a smooth surface matching the nuclear skeleton of the surface atoms). The tip-CNT and CNT-support point contacts when considered are represented by 0.2 nm wide conducting channels. The potential barrier $V(\vec{r})$ is composed of a jellium potential $V_{jell}(\vec{r})$ which models the binding of the electrons in the objects and of the electrostatic potential $V_{elstat}(\vec{r})$ arising from applied STM bias. The jellium potential is zero outside the effective surfaces of the electrodes and -9.81 eV inside.[13] The electrostatic potential is calculated by the capacitance matrix method.[24,25] Although this method is capable of handling the contact potential also, in the present calculation the contact potential is zero because all objects are assumed to have the same material parameters.

III. WAVE PACKET DYNAMICAL CALCULATION OF TUNNEL CURRENT

The quantum mechanical tunneling probability is calculated[13] from the time dependent scattering[26] of a WP on the potential barrier $V(\vec{r})$.

A. Choice of initial wave packet shape

To eliminate the effect of the particular WP shape on the resulting tunneling probability, the WP should have a constant plateau when arriving at the interface region. Using

conventional Gaussian WPs this could be achieved with any desired accuracy by using a lateral spread $\Delta x \gg W_T$ where hW_T is the largest full width at half maximum of the tunneling channel. This approximation was used in Ref. 13 where we modeled a STM measurement having hW_T around 0.1–0.2 nm, a typical minimum achievable value with sharp tips.[20] In the case of CNT rafts, however, the characteristic size of the tunneling region is much larger, which would require the use of a Gaussian WP with fairly large Δx that would subsequently require a fairly large spatial mesh. To avoid this difficulty in the present work, the WP was a *truncated plane wave*, which has a plateau of constant probability density larger than the interface region. Such a WP can be constructed as a convolution of a Gaussian with a square window function. To compensate for the effect of the distortion of the plateau during the time development of the WP a backward time propagator is used to construct the initial state:

$$\psi_0(x,z) = N(a,d_1,d_2)\hat{P}_{t_0} \times \left[\int_{d_1}^{d_2} \exp\left(-\frac{(x'-x)^2}{a^2} + ik_x x \right) dx' \right] \times \exp\left(-\frac{(z-z_0)^2}{a^2} + ik_z z \right), \quad (1)$$

where $d_1 = -1.52$ nm, $d_2 = 1.52$ nm, $a = 0.529$ nm, and N is a normalization constant. By the free space propagator $\hat{P}_{t_0}$ the truncated plane wave is backward propagated in time by an amount $t_0 = (z_0 - z_{interf})/v_z$ where z_0 is the initial z position of the center of the WP, z_{interf} is the z position of the first tunneling interface, and $v_z = k_z$ is the z component of the group velocity. The initial position z_0 was chosen to make the probability density of the initial WP negligible in the interface region.

B. Tunneling probability

The tunneling probability for a given initial WP is determined in the same way as described earlier.[13] Hence only a brief summary of the method is given below. The $\psi(x,z,t)$ time dependent wave function is computed from the time dependent 2D Schrödinger equation by the *split operator Fourier transform method*.[27–29] The probability current density $\vec{j}_{prob}(x,z,t)$ is calculated along a horizontal line (see Fig. 1) inside the tip (support) bulk for tip positive (negative) bias for each time step. Line integration of $\vec{j}_{prob}(x,z,t)$ along this line of constant z gives the probability current $I_{prob}(t)$ and the tunneling probability is $P_{WP}(\vec{k}) = \int_0^{t_{max}} I_{prob}(t)dt$. Calculation is performed until the subsequent change of P_{WP} becomes negligible.

IV. RESULTS

A. Angle dependent transmission for zero bias

Figure 2 shows angle dependent transmission probabilities $P(\theta)$ as a function of the incidence angle θ, which is defined as the angle of the wave vector $\vec{k}_0 = (k_{x0}, k_{z0})$ of the initial WP [cf. Eq. (1)] measured relative to the normal direction (see Fig. 1). Calculations were performed for different number of CNTs: (a) for a STM tunnel junction with no CNT present, (b) for one CNT, and (c) for three CNTs (modeling a CNT raft). In addition we studied the effect of the point contacts in the tip-CNT and CNT-support tunnel junctions. For each barrier the angle dependent transmission was calculated for WPs incident from the support [$P_+(\theta)$, tip positive, solid curves] and for those incident from the tip [$P_-(\theta)$, tip negative, dashed curves]. For these vanishingly small bias calculations the incident WP energy was fixed to $E = E_F = 5$ eV. To check the consistency of the results the angular integral of the transmission probability was calculated for each curve. The integral values for tip positive and tip negative infinitesimal biases were found to agree within 5%, as they should. Because the $P(\theta)$ curves were calculated for only 13 equidistant angle values, we should not expect a better consistency.

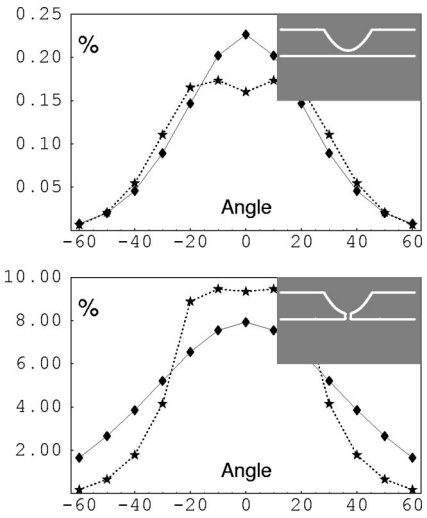

FIG. 2. Transmission probability for the (a) STM tunnel junction with no nanotube present and (b) STM junction shortcut by a point contact. Full (broken) line is for tip positive (negative) case. Model barrier geometry (effective surfaces) is shown in the inset. Note that the vertical scale of the two graphs is different by a factor of 40.

1. Tunneling vs point contact

Figure 2(a) shows the $P_+^{tunnel}(\theta)$ and $P_-^{tunnel}(\theta)$ functions for a STM tunnel junction with no CNT present. $P_+^{tunnel}(\theta)$ will be our reference curve in the following discussion. As we will see in Sec. IV B this curve is very similar to the angular dependence of the tunneling probability for a plane-plane barrier. For increasing angle the tunneling probability decreases because of the decreasing normal momentum of the WP. By contrast, $P_-^{tunnel}(\theta)$ shows a plateau with a shallow minimum around normal incidence. This plateau is caused by the vortices of the probability current density for waves incident from the bulk of the tip.[21,22] The vortices also strongly influence the probability density as shown in Fig. 3. Figure 2(b) shows the influence of a point contact (0.2 nm wide conducting channel) which connects the tip apex to the support. The most obvious effect is the increase of the transmission probability by a factor of about 40. The $P_+(\theta)$ angular dependence is also modified. This is the consequence

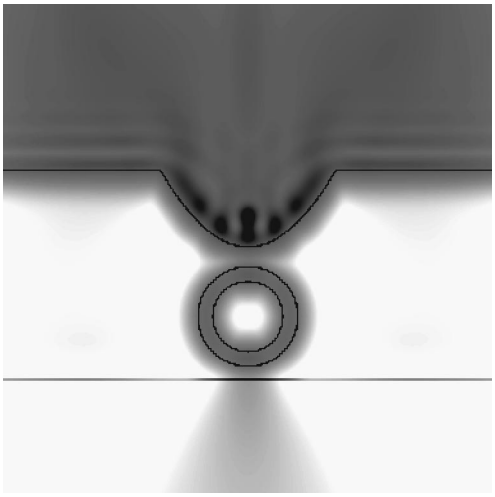

FIG. 3. Influence of probability current vortices inside the tip bulk on the time averaged probability density. The solid dark lines show the effective surfaces of the objects. Width of the presentation window is 5.76 nm. Darker gray shades correspond to larger probability density. A nonlinear gray scale was chosen to facilitate clearer presentation of both the vortices inside the tip and the small density in the support region due to the tunneled-through part of the wave packet.

of switching from tunneling to ballistic flow through the narrow conducting channel. The angular dependence of $P_{-}^{point\ contact}(\theta)$, however, is very similar to the tunneling case apart from the overall increased magnitude. There is a drop of the tunneling probability at around 25° which can be attributed to the narrow aperture angle of the tip. This is simply because WPs incident at large angles from the tip bulk cannot enter the apex. This wave guide effect can be even more pronounced in real experimental situations where the end of the tip has a needlelike shape on the nanometer scale. The functional form of the plateau in $P_{-}^{point\ contact}(\theta)$ is still influenced by the probability vortices inside the tip apex. For small θ values $P_{-}^{point\ contact} > P_{+}^{point\ contact}$ because the tip apex collects the probability waves like a funnel. In the tunneling case this effect is suppressed because these collected waves have a wide angular distribution due to the multiple internal reflections inside the tip apex, and the tunnel effect strongly selects only the normal momentum components in contrast to the point contact where no such self-selection occurs [cf. the $P_{+}(\theta)$ curves for the two cases].

2. Nanotubes in the tunnel gap

In Fig. 4 angle resolved transmission probabilities are shown for one CNT (left graphs) and a CNT raft (right graphs) placed in the STM gap. The raft is modeled by three tubes. In the upper row there is no point contact, in the middle row there is a point contact between the tip and the tube(s) and the lower row shows a situation with point contacts between both the tip and tube(s), and between the tube(s) and its support. The main functional form of $P_{-}(\theta)$ is similar in each case. This is so because P_{-} is mainly determined by the details of the tip apex shape. We have also performed calculations for a point contact only between the tube(s) and the support, a situation not likely to be found experimentally but needed in separating the effects in the case of two point contacts. These results are not shown here because it was found that the shape of $P_{+}(\theta)$ is similar to the two point contact case and only the absolute magnitude is smaller. The functional forms of the upper (no point contact) and middle (tip-tube point contact) P_{+} graphs are also similar apart from a multiplicative factor. This is because the WP travels through two constrictions and the angular dependence of the transmission is mainly determined by the first it passes through. Indeed, the CNT through which the WP propagates

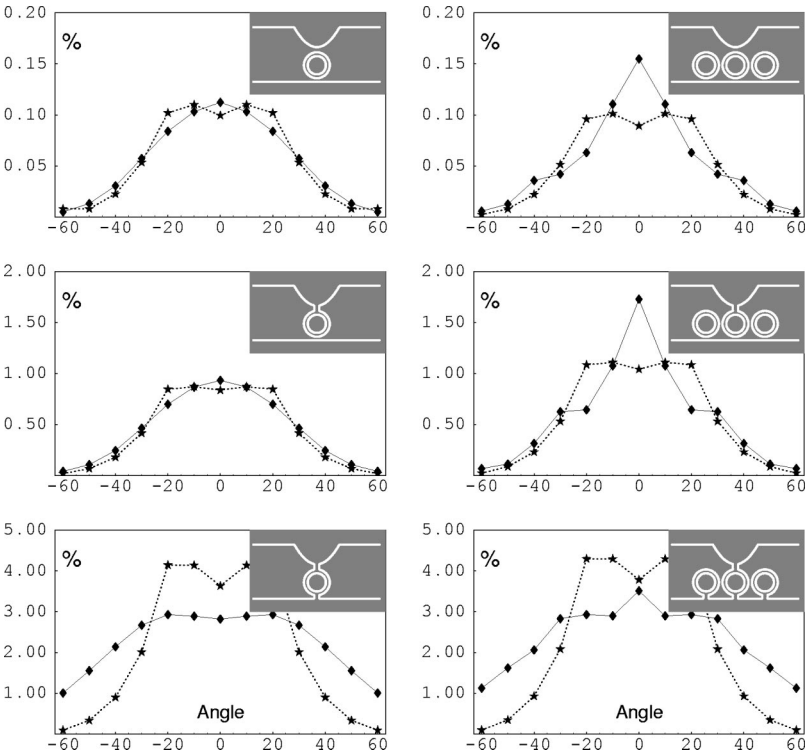

FIG. 4. Transmission probabilities for different numbers of nanotubes and different point contact configurations. Full (broken) line is for tip positive (negative) case. Model barrier geometries (effective surfaces) are shown in the insets. Note the different vertical scale of the graphs, facilitating clearer presentation.

widens the angular wave vector distribution of the WP. We can say that the wave barely remembers its original incidence angle by the time it reaches the second junction. This reasoning explains why the point contact specific angular dependence (cf. Sec. IV A 1) shows up only in the case of tube(s)-support point contact but not for the tip-tube(s) point contact, where a tunneling specific angular dependence remains even though one of the constrictions is actually a point contact.

The $P_+(\theta)$ functions for the raft model (Fig. 4, right panels) have a diffraction-grating-like characteristic shape for all point contact arrangements. We can observe a strong peak around the normal incidence and smaller shoulders around 30°–40°. This diffraction-grating-like behavior is caused by interference between the resonant states of the individual tubes. In a real 3D case this behavior is probably less significant for metallic CNTs, than for semiconducting CNTs because the charge can spread along the metallic CNT easily and this reduces the resonant character of the states on the CNT.

B. Effective tunnel distances

To gain better insight into the results presented in the previous subsections, it is instructive to compare our 2D transmission probabilities with those for a simple plane-plane (1D) case. With the help of the plane-plane model an *effective tunnel distance* d_{eff} will be defined.

The plane-plane tunneling can be solved as a 1D problem.[30] The tunneling probability for a 1D WP with $k_0 > 0$ is

$$P_{1D} = \int_0^\infty |\varphi_0(k,k_0,a)T(k)|^2 dk, \tag{2}$$

where k_0 and a are the mean wave number and width of the initial WP, $\varphi_0(k,k_0,a)$ is the momentum representation of the initial WP and $T(k)$ is the transmission coefficient of the 1D barrier. A step potential (cf. Sec. II) is defined by its height V_0 and width d. This means that P_{1D} is uniquely characterized by the variable set $\{k_0,a,V_0,d\}$ for this type of barrier.

If the WP is incident on a plane-plane barrier not from the normal but from an oblique direction then its transmission probability is determined by the normal component k_{z0} of its wave vector $\vec{k}_0=(k_{x0},k_{z0})=(k_0\sin\theta,k_0\cos\theta)$. Due to the constant potential in the region from which the WP is launched, we may write the translational kinetic energy of the WP as $E_0=|\vec{k}_0|^2/2=k_{x0}^2/2+k_{z0}^2/2$. So we can define its transverse and normal translational kinetic energy components by

$$E_0 = E_{x0}+E_{z0} = E_0\sin^2\theta + E_0\cos^2\theta. \tag{3}$$

The transmission probability of the plane-plane barrier depends only on the E_{z0} normal energy component of the WP:

$$P_{plane\text{-}plane}(E_0,\theta,a,V_0,d) = P_{1D}(E_{z0},a,V_0,d). \tag{4}$$

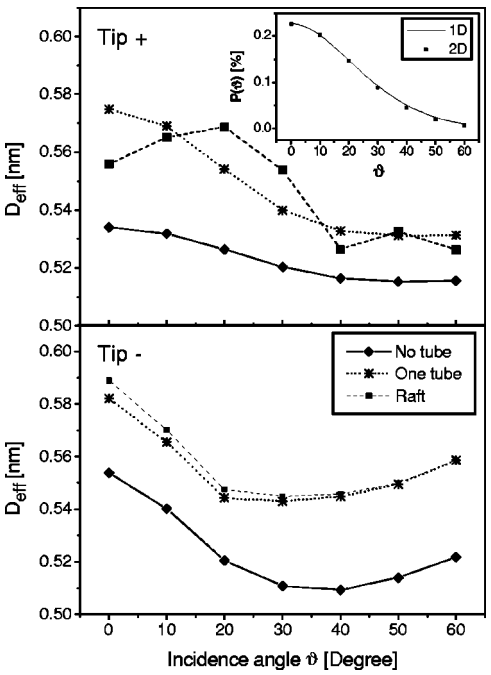

FIG. 5. Effective tunnel distances for different number of nanotubes and for (a) tip positive and (b) tip negative cases. Inset: the points are the calculated $P_+(\theta)$ values for different angles [same curve as on Fig. 2(a)]. The solid line is the transmission for a wave packet incident from the *normal direction* with $E_0=5\cos^2\theta$ eV energy. See the text for details.

Using this formulation we can associate with any transmission function $P_{2D}(E_0,\theta)$ a (generally energy and angle dependent) effective tunnel distance $d_{eff}(E_0,\theta)$ by the equation

$$P_{2D}(E_0,\theta) = P_{1D}(E_0\cos^2\theta,a,V_0,d_{eff}). \tag{5}$$

Figure 5 shows the $d_{eff}(\theta)$ functions for different STM situations. d_{eff} is a nearly constant 0.52 nm for the STM tunnel junction with no CNT present at an infinitesimal tip positive bias. This tells us that the barrier consisting of a plane and a hyperbolic tip with 0.5 nm radius at 0.409 nm distance is approximately equivalent for WPs defined in Sec. III A to a plane-plane barrier with $d_{eff}=0.52$ nm. This constant value of the effective tunnel distance is a justification for using a 1D model for describing the functioning of the STM in front of a flat surface. The reason behind this is the negligible mixing of the normal and transverse momentum components. This separability of the momentum components is further demonstrated in the inset of Fig. 5. The points are the calculated $P_+(\theta)$ values for different angles [the same curve as on Fig. 2(a)]. The solid line is the transmission for a WP incident from the *normal direction* with $E_0=5\cos^2\theta$ eV energy. The good match of these two curves shows that tunneling through this barrier is only negligibly influenced by the transversal momentum.

All other d_{eff} curves of Fig. 5 show a considerable angle dependence, which is the effect of the larger normal-transverse momentum mixing. In the case of the $P_-(\theta)$ curves this mixing is largely dominated by the vortices inside the tip apex. Hence functional forms of $P_-(\theta)$ curves are very similar to each other independently of the presence and

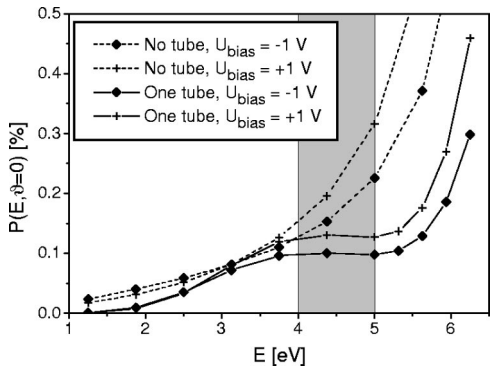

FIG. 6. Energy dependent transmission of a wave packet incident from the normal direction for tip positive and tip negative 1 V bias potential. Full (broken) lines are for one (zero) nanotube. The zero of the energy scale is fixed at the band bottom of the *launching side* of the wave packet. On this energy scale the states between $E=4$ eV and $E=5$ eV (shaded region on the figure) always contribute to the tunnel current at zero temperature.

number of CNTs in the junction. The presence of CNT(s) introduces only a constant shift in d_{eff} of about 0.027 nm, although the tip-support distance is increased by 1.335 nm by inserting the CNTs. For tip positive infinitesimal bias, however, the transmission of the raft is markedly different from that of the single tube: the diffraction-grating-like behavior that was already discussed in Sec. IV A 2 is clearly visible.

C. Tunneling with nonvanishing bias

To model the nonvanishing bias an electrostatic potential calculated by the capacitance matrix method[24,25] was added to the jellium potential. The sign of the potential was always set in agreement with the WP incidence direction, i.e., the WP was always launched opposite to the electric field, $\vec{E}\cdot\vec{k}_0<0$. For a positive (negative) tip the WP was always launched from the support (tip). Thus different potentials are experienced by the WPs coming from the two directions; hence the angular integrals of $P_+(\theta)$ and $P_-(\theta)$ need no longer be equal and this causes an asymmetry in the calculated $I(V)$ curves. All three objects [tip, CNT(s), and support] are assumed to be perfect conductors for the electrostatic field calculation. For metallic CNTs this is a plausible assumption because of their small screening length.[31,32] In nonmetallic tubes the electrons cannot move freely along the tube axis. Thus our perfectly conducting ring model is valid for the semiconducting tubes if only the electrons can move freely along the circumference of the tube. The $U_{support}$ and U_{tip} potentials are fixed by the STM setup: $U_{support}=0, U_{tip}=U_{bias}$.

The U_{tube} potential was determined by assuming charge neutrality. This condition gives $U_{tube}=0.376U_{bias}$ for the single CNT and $U_{tube}=0.288U_{bias}$ for the CNT raft.

1. Energy dependence of transmission

Figure 6 shows the incidence energy dependence of the transmission probability of WPs with normal incidence through a STM tunnel junction with no CNT present and through a CNT for tip positive and tip negative 1 V biases. The zero of the energy scale is fixed at the bottom band of the *launching side* of the WP for both polarities. On this energy scale the states between $E=4$ eV and $E=5$ eV (shaded region on the figure) contribute to the tunnel current at zero temperature. The transmission for the STM tunnel junction with no CNT present follows an exponential-like energy dependence characteristic of plane-plane tunneling (cf. Sec. IV B). The presence of a CNT, however, causes a plateau to appear between 3.8 and 5 eV. This plateau is a sign of resonant tunneling[13] caused by the two tunnel interfaces.[12]

2. Tunnel current calculation

To estimate the tunnel current flowing through a real 3D junction we have to make some assumptions about the behavior of the system in the direction perpendicular (y direction) to our 2D calculation plane (xz plane). To this end, we have used the following simple approximations. (i) The y diameter of the tunneling channel at the tip apex is assumed to be a constant 0.2 nm. (ii) The transmission is assumed to depend on the in-plane and perpendicular-to-the-plane angles independently. (iii) The perpendicular-to-the-plane angle dependence is taken to be the same as that of a plane-plane system (see Sec. IV B).

After calculating the total 3D $P(U_{bias},\vec{k})$ transmission probability in the above approximation, the tunnel current is

$$I(U_{bias})=\frac{1}{4\pi^3}A_{WP}^{eff}\int_{\text{allowed}}P(U_{bias},\vec{k})k_z d\vec{k},$$

where A_{WP}^{eff} is the effective lateral (xy) area of the WP defined as

$$A_{WP}^{eff}=\frac{1}{\left(\int_{-\infty}^{+\infty}\rho_{WP}(x_0,z,t=0)dz\right)^2}$$

and x_0 is the initial x position of the center of the WP.

Assuming a free-electron-like $E(\vec{k})$ relation and density of states (DOS), the allowed $\vec{k}$ space region is the region between the $E=E_F$ and $E=E_F-U_{bias}$ hemispheres. $I(U_{bias})$ curves for the STM tunnel junction with no CNT present, for one CNT, and for three CNTs are shown in Fig. 7(a).

The absolute value of the current is higher than those measured in typical STS experiments. This is partly an artifact of the WP dynamical method attributed to the amplification effect[33] of the higher momentum components in the tunneling process. Further, experimental aspects of this higher than usual tunnel current are given in Sec V below.

All $I(U_{bias})$ curves of Fig. 7(a) show some degree of asymmetry. These asymmetries are better displayed in the $I(U_{bias})+I(-U_{bias})$ graphs of Fig. 7(b). Note that, while the asymmetry of the STM tunnel junction with no CNT present shows a linear U_{bias} dependence and its magnitude is only 2.5%, the asymmetry of the tunnel gaps with CNTs increase with U_{bias} and reach a value of more than 20% at 1 V bias. It should be emphasized that these asymmetries are of pure geometrical origin because of the free-electron-like DOS assumption.

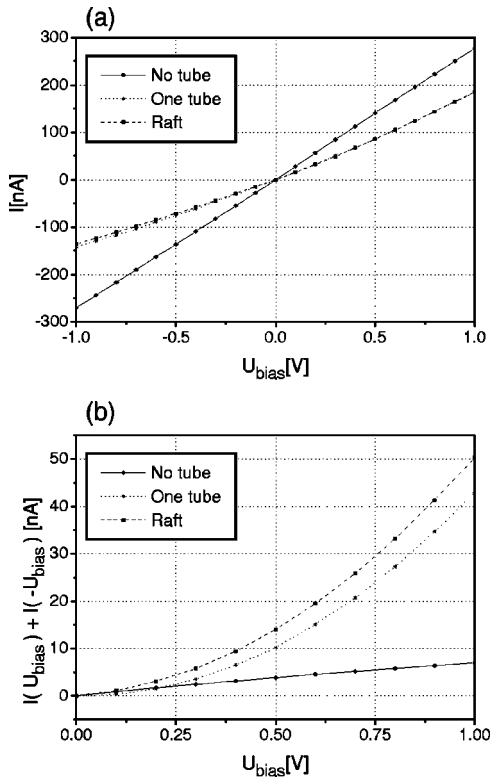

FIG. 7. (a) Tunnel current as a function of applied bias for a STM tunnel junction with no nanotube present, for one nanotube, and for a nanotube raft. (b) Tunnel current asymmetries for the curves in (a).

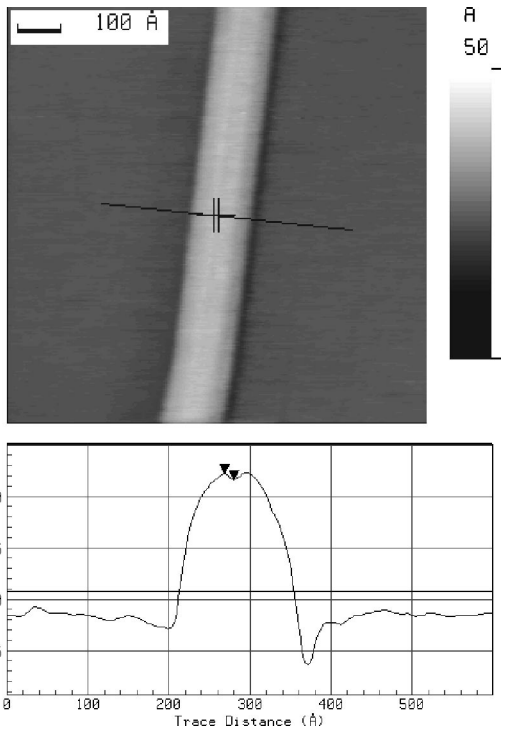

FIG. 8. Constant current topographic STM image of a MWCNT on HOPG, $I_t = 1.02$ nA, $U_g = 100$ mV. The line cut shown runs along the black line in the image; the two crosses label the positions of the markers shown in the line cut.

V. DISCUSSION

The experimental STS curves[7–11] of CNTs frequently show some degree of asymmetry with respect to bias voltage polarity. In some cases this asymmetry has been attributed to charge transfer between the Au substrate and the CNT.[7] Asymmetry was observed in STS measurements of CNTs on HOPG,[9,11] too, where charge transfer should be very limited. The degree of asymmetry is a variable quantity even for measurements reported within the same paper. According to the simulation results presented above, two possible reasons for asymmetry in the STS data are as follows: (i) effects arising from the particular tip geometry, (ii) effects arising from point contact during imaging and/or during STS measurements. The very end of an STM tip may have a shape that deviates drastically from the idealized geometry used in our model. However, a more complex tip may be generated by considering the tip as being composed of several idealized tips. This kind of approach was used earlier for analyzing multiple tip effects[34,35] in atomic resolution STM images. In the framework of our model it follows from this approach that the particular tip shape will influence the structure of the vortices produced in the tip and by this can modify the particular shape of the $P_-(\theta)$ function. This kind of effect is expected to influence the negative side of the STS curve when positive polarity means tunneling from sample to tip. Due to the fact that the tip acts like a ''waveguide,'' the width/length ratio of the active microtip, i.e., of the tip that is really responsible for the tunneling, may also have a role in deciding the characteristic vortex structure. The second kind of asymmetry source is the point contact between the CNT and its support; in fact, this means that there are two point contacts: one at the STM tip/CNT interface—this will influence the magnitude of the tunneling current—and the second one at the CNT/support interface. This latter one is produced by pressure exerted by the STM tip on the top of the CNT. Recent theoretical arguments suggest that differences in the electronic structure of the CNT and of the metal that is within tunneling distance may introduce an additional energy barrier of 10 eV.[36] This may lead to reduction of the tunneling gap over the CNT and to compression of the CNT between the STM tip and the support. The second point contact (CNT/support) will introduce asymmetry in the STS spectra. In this case unusual features are expected on the positive side of the STS spectrum when tunneling takes place from sample to tip, while the negative side will not differ in shape from symmetric spectra but the magnitude of the tunneling current will increase significantly. These expectations are fulfilled by the experimental data reported in Ref. 11. This second kind of asymmetry is expected to show up in those STS measurements for which larger tunneling current values were used while establishing the position of the STM tip before the feedback loop was switched off. If the transmission through the system STM tip/CNT/support is low, then during the constant current imaging operation (when the width of the tunneling gap used during the STS measurement is also determined) the tip can come into mechanical contact with the topmost part of the CNT. When this occurs, the topographic image will not be drastically altered. The compression effects may be visible in transverse line cuts taken across the CNT like the one shown in Fig. 8. Although it may affect the image quality, the point contact will not impede achieving atomic resolution imaging, as in Fig. 9, taken at a slightly

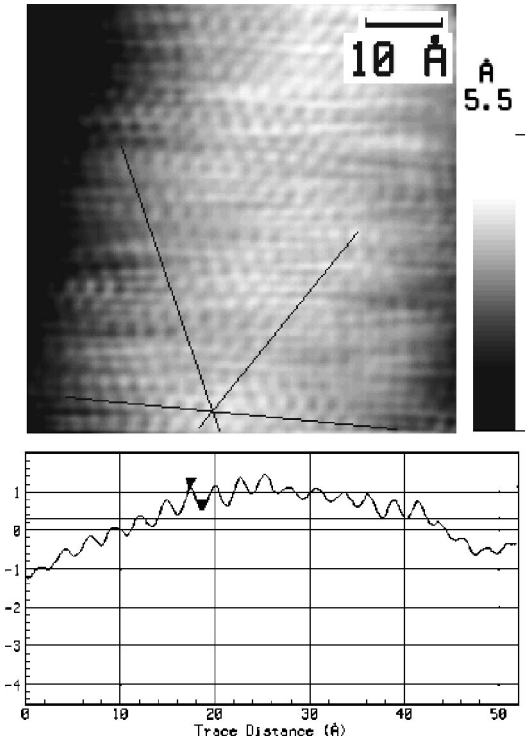

FIG. 9. Atomic resolution, constant current, topographic image taken on the topmost region of the carbon nanotube shown in Fig. 8. $I_t = 1.0$ nA, $U_g = 100$ mV. Note the three lines oriented along the the directions in which the β sites (visible in the STM images of graphite) are aligned. The line cut clearly shows the curvature of the nanotube and the atomic corrugation. Some blurring is present in the image due to the mechanical contact of the tip with the nanotube.

smaller tunneling current as compared with Fig. 8. This is in agreement with earlier point contact atomic resolution achieved on HOPG.[15] These findings show that topographic STM images and STS curves are best accompanied by line cuts taken across the CNT investigated. Frequently, current imaging tunneling spectroscopy (CITS) is used to acquire spectroscopic data in several (or every) pixel points that compose a STM image. When performing CITS the feedback loop is switched on and off for every pixel, but, again, the value of the STM gap is selected during the acquisition of the topographic information. It may happen that for different points of the image the width of the tunneling gap will be different, as in the case of rafts of CNTs.[11] If this happens symmetric and asymmetric STS curves may be measured over the same CNT. Beyond the effects arising from point contact, it follows from Fig. 5 that the particular arrangement of the CNTs in a raft or a bundle will leave its fingerprint on the shape of the STS curves.

As we noted in Sec. IV C 2, the absolute values of our calculated currents are higher than those in STS measurements. In STM experiments the tunneling gap is determined in topographic mode. This means that a 1 nA current is expected at, say, 0.1 V bias at a gap of 0.4 nm. Now, when U_{bias} is increased without modifying the gap value—which does not happen during normal, topographic imaging, because the feedback loop would correct it automatically—it results in a strong increase of the tunneling current. This is the reason, when doing spectroscopy, for choosing a ''starting gap'' large enough that at the edges of the voltage range the allowable current limit of the electronics is not exceeded. Furthermore, if a certain energy density is exceeded in the tunneling channel, then permanent modifications of the sample and/or tip structure may occur, which will alter the shape of the spectroscopic curve.

VI. CONCLUSION

We have calculated incidence angle and energy dependent wave packet transmission coefficients through a STM junction model containing various configurations of carbon nanotubes. From the 2D scattering calculated from the time dependent Schrödinger equation, 3D transmission coefficients are derived by assuming no mixing of the wave packet momentum components along the tube axis and perpendicular to the tube axis. The total tunnel current at a given bias is calculated by the statistical average of probability currents for all wave packets, assuming a free electron dispersion relation.

It was found that for tip negative bias (the wave packet approaching the tunnel junction from the tip) the angular dependence of the transmission is mainly determined by the tip shape. The particular tip shape determines the probability current vortices inside the tip and this effect introduces an asymmetry on the negative side of the STS spectrum.

For tip positive bias (the wave packet approaching the tunnel junction from the support), however, the angular dependence of the transmission depends strongly on the nature of the nanosystem placed in the STM gap. The tip positive transmission of a STM tunnel junction with no nanotube present can be well represented by a plane-plane model, while all other configurations studied show a considerable amount of normal-transverse momentum mixing. The angular dependence of the transmission of the nanotube raft shows a diffraction-grating-like behavior.

Point contacts between the nanotube and its support caused by mechanical pressure exerted by the STM tip cause an asymmetry to appear on the positive side of the STS spectrum.

To our knowledge the present calculation is the first to yield tunnel current directly comparable to experimental data for carbon nanotubes. While for a STM tunnel junction with no nanotube present the calculated STS spectrum shows only a small linear in U_{bias} asymmetry, for nanotubes there are considerable degrees of asymmetry present in the $I(V)$ curves. Because of the free electron DOS assumption these asymmetries are of purely geometrical origin.

ACKNOWLEDGMENTS

This work was supported by the Belgian Federal OSTC PAI-IUPAP P4/10 program and the Hungarian OTKA Grant No. T 30435. G.I.M. and L.P.B. gratefully acknowledge a grant from the Belgian Federal OSTC and hospitality at FUNDP, Namur.

*Email address: mark@sunserv.kfki.hu

[1] J.W. Mintmire, B.I. Dunlap, and C.T. White, Phys. Rev. Lett. **68**, 631 (1992); R. Saito, M. Fujita, G. Dresselhaus, and M.S. Dresselhaus, Appl. Phys. Lett. **60**, 2204 (1992).

[2] J.-C. Charlier and Ph. Lambin, Phys. Rev. B **57**, R15 037 (1998).

[3] M. S. Dresselhaus, G. Dresselhaus, and P. C. Eklund, *Science of Fullerenes and Carbon Nanotubes* (Academic Press, San Diego, 1996).

[4] A. Thess, R. Lee, P. Nikolaev, H. Dai, P. Petit, J. Robert, C. Xu, Y.H. Lee, S.G. Kim, A.G. Rinzler, D.T. Colbert, G.E. Scuseria, D. Tománek, J.E. Fischer, and R.E. Smalley, Science **273**, 483 (1996).

[5] L.P. Biró, S. Lazarescu, Ph. Lambin, P.A. Thirty, A. Fonseca, J.B. Nagy, and A.A. Lucas, Phys. Rev. B **56**, 12 490 (1997).

[6] W. Clauss, Appl. Phys. A: Mater. Sci. Process. **69**, 275 (1999).

[7] J.W.G. Wildöer, L.C. Venema, A.G. Rinzler, R.E. Smalley, and C. Dekker, Nature (London) **391**, 59 (1998).

[8] T.W. Odom, J.-L. Huang, Ph. Kim, and Ch.M. Lieber, Nature (London) **391**, 62 (1998).

[9] D.L. Carroll, P. Redlich, P.M. Ajayan, J.C. Charlier, X. Blase, A. De Vita, and R. Carr, Phys. Rev. Lett. **78**, 2811 (1997).

[10] A. Hassanien, M. Tokumoto, Y. Kumazawa, H. Kataura, Y. Maniwa, S. Suzuki, and Y. Achiba, Appl. Phys. Lett. **73**, 3839 (1998).

[11] L.P. Biró, P.A. Thiry, Ph. Lambin, C. Journet, P. Bernier, and A.A. Lucas, Appl. Phys. Lett. **73**, 3680 (1998).

[12] L.P. Biró, J. Gyulai, Ph. Lambin, J.B. Nagy, S. Lazarescu, G.I. Márk, A. Fonseca, P.R. Surján, Zs. Szekeres, P.A. Thiry, and A.A. Lucas, Carbon **36**, 689 (1998); http://www.phy.bme.hu/pub/emrs97/index.html.

[13] G.I. Márk, L.P. Biró, and J. Gyulai, Phys. Rev. B **58**, 12 645 (1998).

[14] R. Wiesendanger, *Scanning Probe Microscopy and Spectroscopy* (Cambridge University Press, Cambridge, 1994).

[15] N. Agrait, J.G. Rodrigo, and S. Vieira, Ultramicroscopy **42-44**, 177 (1992).

[16] R.M. Feenstra, J.A. Stroscio, and A.P. Fein, Surf. Sci. **181**, 295 (1987).

[17] V. Meunier and Ph. Lambin, Phys. Rev. Lett. **81**, 5588 (1998).

[18] L.C. Venema, V. Meunier, Ph. Lambin, and C. Dekker, Phys. Rev. B **61**, 2991 (2000).

[19] N. Barniol, F. Pérez, and X. Aymerich, J. Vac. Sci. Technol. B **9**, 483 (1991).

[20] A.A. Lucas, H. Morawitz, G.R. Henry, J.-P. Vigneron, Ph. Lambin, P.H. Cutler, and T.E. Feuchtwang, Phys. Rev. B **37**, 10 708 (1988).

[21] Th. Laloyaux, A.A. Lucas, J.-P. Vigneron, Ph. Lambin, and H. Morawitz, J. Microsc. **152**, 53 (1988).

[22] Th. Laloyaux, I. Derycke, J.-P. Vigneron, Ph. Lambin, and A.A. Lucas, Phys. Rev. B **47**, 7508 (1993).

[23] D. Östling, D. Tománek, and A. Rosén, Phys. Rev. B **55**, 13 980 (1997).

[24] A. Sommerfeld, *Electrodynamics* (Academic Press, New York, 1996), p. 70.

[25] S.J. Beard and R.W. Hockney, Comput. Phys. Commun. **36**, 25 (1985).

[26] M.C. Yalabik, G. Neofotistos, K. Diff, H. Guo, and J.D. Gunton, IEEE Trans. Electron Devices **36**, 1009 (1989).

[27] J.A. Fleck, J.R. Morris, and M.D. Feit, Appl. Phys. **10**, 129 (1976).

[28] M.D. Feit, J.A. Fleck, and A. Steiger J. Comput. Phys. **47**, 412 (1982).

[29] G. I. Márk and P. Pacher, in *Proceedings of the International Conference on Mathematical Methods in Science and Technology, 1995, Vienna*, edited by W. Kainz (University of South Bohemia, Českě Budejovice, 1995), p. 59.

[30] C.R. Leavens and G.C. Aers, Phys. Rev. B **39**, 1202 (1989).

[31] M.F. Lin and D.S. Chuu, Phys. Rev. B **56**, 4996 (1997).

[32] Ch. Girard, M. Devel, X. Bouju, and P.A. Gravil, in *Atomic and Molecular Wires*, Vol. 341 of NATO Advanced Study Institute, Series E Applied Science, edited by C. Joachim and S. Roth (Kluwer, Dordrecht, 1997), p. 179.

[33] G. I. Márk, in *Tunneling and its Implications*, edited by D. Mugnai, A. Ranfagni, and L. S. Schulman (World Scientific, Singapore, 1997), p. 443.

[34] H. Mizes, S.-I. Park, and W.A. Harrison, Phys. Rev. B **36**, 4491 (1987).

[35] L. P. Biró, G. Márk, and E. Balázs, in *Nanophase Materials*, Vol. 260 of *NATO Advanced study Institute Series, E*, edited by G. C. Hadjipanayis and R. W. Siegel (Kluwer, Dordrecht, 1994), p. 205.

[36] J. Tersoff, Appl. Phys. Lett. **74**, 2122 (1999).